MHz - Tomoscopy

D3.4

Report on sample experiment, data evaluation, and validation of the method

Project information

Project full title	MHz rate multiple projection X-ray Microscopy
Project acronym	MHz-TOMOSCOPY
Grant agreement no.	101046448
Instrument	EIC Pathfinder Open
Duration	42 months
Website	https://tomoscopy.eu/

Deliverable information

Deliverable no.	D3.4
Deliverable title	Report on sample experiment, data evaluation, and validation of the method
Deliverable responsible	UOXF
Related Work-Package/Task	Task 3.4
Type (e.g. report; other)	Report
Author(s)	Mohammad Shahsavari and Daniel Eakins
Dissemination level	public

Funded by
the European Union

Document Version	1.0
Date	11/27/2025
Download page	

Document information

Version no.	Date	Author(s)	Comment
1.0	11/27/2025	Mohammad Shahsavari and Daniel Eakins	-

Funded by
the European Union

Abstract

In Task 3.4, we focused on finalising the sample environment for the sample experiment to validate the MHz-TOMOSCOPY technique. This has been achieved by carrying out both numerical simulations and in-house experiments at the University of Oxford and experiments at the EuXFEL using the SPB/SFX X-ray instrument. This document provides a concise summary of the studied sample environments and the corresponding experimental and numerical results for designing a suitable sample environment for MHz-TOMOSCOPY. It also reports the obtained results using the MHz rate multiple projection X-ray microscopy technique developed in this project.

Executive Summary

In D3.4, we report on the sample environment and experiments to validate the MHz rate multiple projection X-ray microscopy technique developed in WP1. This includes detailing the key selection criteria, associated experiments, and the methodology used to evaluate these criteria. In this deliverable, we also present the results obtained by utilising the technique, followed by our forthcoming studies beyond this project.

Funded by
the European Union

Table of Contents

Funded by
the European Union

Introduction

In this project, we chose to visualise cavitation for validating the MHz rate multiple projection X-ray microscopy (MHz-TOMOSCOPY) technique developed in WP1. This physical phenomenon refers to the formation of vapour in a liquid when the fluid flow pressure drops below the saturated pressure [1]. Cavitation involves a significant density gradient in the flow [2], making it a suitable sample environment for the visualisation using X-ray imaging techniques, including the MHz-TOMOSCOPY. Furthermore, despite extensive efforts to understand various aspects of cavitation in the past, many of these aspects have not been precisely explored yet. This is mainly because cavitation involves complex physical phenomena at the microscale level, which are not accessible with conventional visualisation techniques, namely Shadowgraph and Schlieren [3]. Given the broad range of applications of cavitation in science and engineering, e.g. in pharmaceutical [4], biomedical science [5, 6], water treatment [7, 8], and material science [9], exploring cavitation using the novel MHz-TOMOSCOPY provides new insights to understand and optimise cavitation devices to improve the cavitation based processes in the applications mentioned above.

In Task 3.4, we focused on designing a sample environment and performing experiments on it to both validate the MHz-TOMOSCOPY technique and explore the unknown features of cavitation, providing a broad range of cavitation applications with a new wealth of knowledge. To achieve this goal, we established specific criteria—outlined in this report—to effectively leverage the unique capabilities of MHz-TOMOSCOPY. Using this well-structured approach, we also identified and overcame challenges in applying the technique to visualise cavitation through the combination of preliminary numerical simulations and in-house experiments at the University of Oxford, as well as selected experiments using the SPB/SFX X-ray instrument at the EuXFEL. This approach can also be extended to other future applications of MHz-TOMOSCOPY.

In this report, we briefly introduce our methodology, the criteria, the investigated sample environments, and the obtained results on the most suitable sample environment for MHz-TOMOSCOPY.

Methodology

The numerical simulations for designing the sample environment and experiments were performed using the cost-efficient and advanced code developed in WP3. The details of these codes were presented in D3.2. Furthermore, the experimental investigations were conducted using a cavitation apparatus shown schematically in Fig. 1. The apparatus consisted of a hydraulic loop and sample environments, coupled with the shadowgraph imaging technique at the University of Oxford and the SPB/SFX X-ray instrument at the EuXFEL. In the hydraulic loop, a pump was used to circulate water in the loop, and the flow pressure was measured using two sets of pressure indicators and transmitters on the sides of the sample environment. The uncertainty and repeatability of the pressure transmitters were less than ±0.25% and ±0.1% of the 4-bar full-scale range, respectively. Moreover, a valve was used downstream of the sample environment to adjust the back pressure. The water flow rate was measured using a turbine flow transmitter with an accuracy of ±2% and repeatability of ±1% of the full-scale range. The fluid temperature was measured using a type T thermocouple with an accuracy of ±0.1 °C. A NI DAQ

device integrated with LabVIEW software was used to acquire the pressure and flow rate measurements and control the valve.

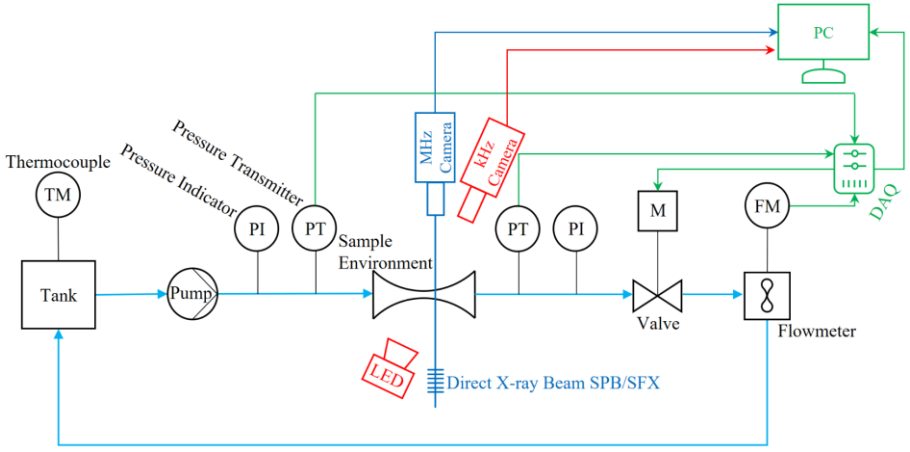

Fig 1. Schematic of the experimental apparatus.

In this apparatus, the shadowgraph imaging technique uses a 120 W LED light source and a high-speed Phantom camera (V7.3) equipped with a Nikon AF Micro lens with a focal length of 60 mm and 32 mm macro extension tubes. The samples were placed between the uniform light source and the high-speed camera. The exposure time, the sampling frequency, and recording time of the camera were set at 1 µs, 20 kHz, and 1 s, respectively. The field of view covered by this technique was 15.36 × 7.68 mm^2, with a pixel size of 30 µm. The SPB/SFX X-ray instrument at the EuXFEL utilises an indirect X-ray microscope with a fast camera to capture images at a MHz repetition rate. This instrument provides X-ray pulses in burst mode with a burst length of 600 µs and a repetition rate of 10 Hz. Each burst contains X-ray pulses at a MHz repetition rate. The MHz camera was synchronised with the burst of X-rays to record 128 frames per burst at a frame rate of 1.13 MHz. The field of view was 1.28 × 0.8 mm^2, and the pixel size was 3.2 µm. The X-ray beam size was 1.5 mm within the sample environment with a photon energy of 10 keV. Further details of the multi-projection method in the MHz-TOMOSCOPY prototype were presented in previous deliverables, i.e., D1.4 and D1.5.

Sample environment criteria

We defined and evaluated a comprehensive set of criteria for designing a suitable sample environment and experiments to validate the MHz-TOMOSCOPY technique, which are listed as follows.

Beam transmission requirement

The EuXFEL provides an X-ray free-electron laser beam into the SPB/SFX X-ray instrument with a typical photon energy of 10 keV and a maximum energy of 25 keV. This limits the amount and type of material in front of the beam to properly visualise a physical phenomenon, particularly when the beam is split in the MHz-TOMOSCOPY technique. Increasing the sample environment size reduces the beam transmission through the sample, decreasing the signal-to-noise and resulting image quality. Moreover, the transmission through some materials is very low, as

illustrated in Fig. 2, which shows the beam transmission through 2 mm of material as a function of photon energy. Figure 2 indicates that the transmission is significantly lower through glass than through PMMA.

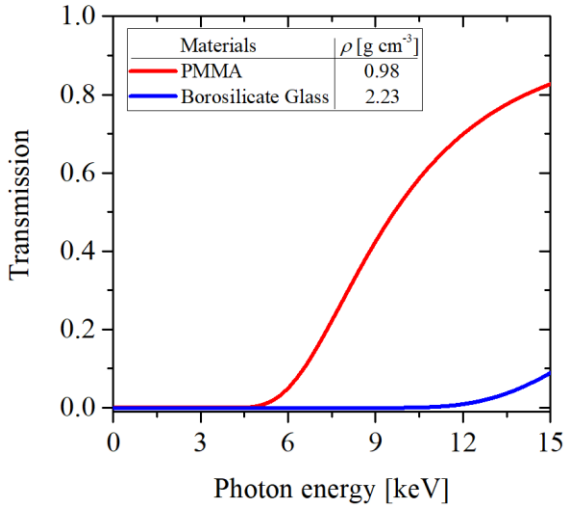

Fig 2. Beam transmission through 2 mm glass and PMMA as a function of photon energy.

Considering the typical value of photon energy in the SPB/SFX X-ray instrument, i.e., 10 keV, a proper visualisation requires at least 0.5 beam transmission. Given these details, it became evident that the original demonstrator application, i.e., wet cavitation peening, would not be well-matched to the capabilities of the technique prototype due to limited beam penetration through both material and fluid, as well as the inability of the technique to capture shock wave propagation in the fluid phase. Therefore, the focus of this work package was shifted toward investigating cavitation. These analyses and the preliminary experiments at EuXFEL showed that the sample environment should include less than 2 millimetres of solid material, preferably PMMA (as illustrated in Fig. 2), and fluid to visualise cavitation.

Novelty requirement

Another important criterion considered in this work is the novelty of the research topic. Although the primary objective of this project is to develop and validate an advanced 4D visualisation technique, the sample environment and the experiment output should be scientifically relevant and novel for engineering applications. To meet this requirement, we performed a comprehensive literature review to identify knowledge gaps in various cavitation applications that can be addressed with the MHz-TOMOSCOPY technique. These gaps are outlined below and depicted in Fig. 3:

- Coherent motions in hydrodynamic cavitation

  Hydrodynamic cavitation refers to the formation of vapour cavities in liquids when the local liquid pressure drops below the saturated pressure due to the flow acceleration [1]. This class of cavitation has been widely exploited to harness the energy generated during cavitation bubbles across different processes [10-13]. Recent studies indicated that coherent turbulent motions, including vortex and spiral structures, play a significant role in enhancing the performance of processes [14-18]. Figure 3 (a) illustrates an example of such coherent motions: water flows from left to right through a venturi tube, while upstream

swirl generates coherent, spiral-shaped cavitating structures. However, there is still no explicit explanation for such performance enhancements in hydrodynamic cavitation applications.

- Bubble-induced cavitation

  Recent studies indicate that introducing gas bubbles into the liquid flow can promote cavitation, enabling a well-controlled cavitation process [19, 20]. In this process, cavitation is initiated at the gas bubble-liquid interface, accompanied by interface instabilities. This is illustrated in Fig. 3 (b) for a slug venturi flow obtained by using shadowgraph imaging at the University of Oxford. Moreover, previous studies have shown that the existence of gas bubbles in liquid can expedite cavitation and reduce power consumption [20, 3]. However, these bubbles reduce the energy release by cavitation collapse significantly [21, 22]. The MHz-TOMOSCOPY technique is a unique method for visualising the multi-way interactions between gas, vapour, and liquid phases, which have not been well-understood yet. These details can inform modifications to this class of cavitation to enhance the energy harnessed from cavitation bubble collapse.

- Laser-induced cavitation

  Another effective method to precisely control cavitation features is to generate cavitation bubbles via laser discharges [2, 23]. Similar to bubble-induced cavitation, this process also involves fast-forming features that are not accessible with conventional imaging techniques [24]. We performed preliminary studies using the CFD solvers detailed in D3.2 to characterise the spatiotemporal features of laser-induced cavitation, and a snapshot of the obtained results is shown in Fig. 3 (c). In this figure, the maximum size of the bubble generated by the laser discharge is shown by the black solid line, while the white line shows the bubble shape at the onset of the collapse. The left part of the figure shows the spatial distribution of the pressure normalised by the ambient pressure, and the spatial distribution of the velocity field is shown on the right-hand side of the figure.

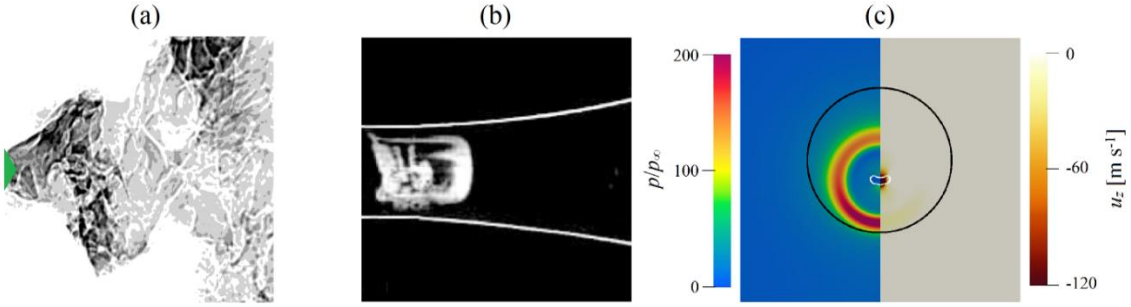

Fig 3. Snapshots of (a) coherent motions in hydrodynamic cavitation obtained by using the SPB/SFX X-ray instrument, (b) bubble-induced cavitation obtained by using shadowgraph imaging at the University of Oxford, and (c) laser-induced cavitation from numerical simulations.

Resolution requirement

One of the most crucial criteria in selecting the sample environment is matching the spatiotemporal resolution of the MHz-TOMOSCOPY technique with the cavitation time and length scales. As detailed in the "Methodology" section, the MHz-TOMOSCOPY technique records 128 frames with a recording speed of 1.1 million frames per second, covering a duration

of 116 us. Moreover, the field of view of this technique is 1.28 × 0.8 mm^2. Employing the numerical and experimental techniques detailed in the "Methodology" section, we estimated the required recording duration and field of view to visualise cavitation in the potential sample environments listed in the previous section. Figure 4 compares these requirements with the MHz-TOMOSCOPY's resolutions. The results show that visualising the coherent motions in hydrodynamic cavitation requires a significantly large field of view and recording duration, which are not achievable using the technique. Although the recording duration of the technique matches that required to study bubble-induced cavitation, this sample environment demands a large field of view to cover the evolution of the cavitating regions near a gas bubble. This is because the gas bubble and the subsequent features are not spatially stationary in the flow. However, the required field of view and recording duration for laser-induced cavitation are very controllable and can be adjusted precisely by manipulating the laser energy and its spot size. Numerical simulations show that the required spatiotemporal resolution for this sample perfectly matches the technique resolution for sub-millimetre laser-induced bubbles.

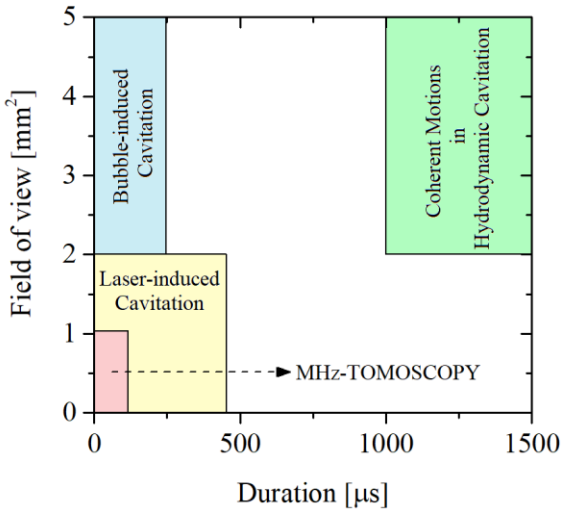

Fig. 4. Field of view and recording duration required to study cavitation in the selected configuration compared to the MHz-TOMOSCOPY technique's resolution.

Numerical simulation requirement

An additional requirement of the sample environment is that the cavitation features should be reproducible using the CFD solvers developed in this project. Validations of these solvers, introduced in D3.2, have shown that the developed numerical platforms can well predict coherent motions in hydrodynamic cavitation and laser-induced cavitation. Nevertheless, simulating the bubble-induced cavitation requires further model adjustments.

Designed sample environment

Considering the criteria presented in the previous section, we concluded that studying cavitation in the laser-induced bubble configuration is both fundamentally interesting for the engineering communities and feasible using the MHz-TOMOSCOPY technique. Based on these analyses and considering the technique limitations, we designed a rectangular tube to study laser-seed cavitation, with inner dimensions of 1.9 (width) × 1.9 (height) × 12 (length) mm^3. To minimise the

shock wave reflections from the far-field boundary condition, we used a long tube with a length of 12 mm connected to a 1 m tube. The dimensions of the tube cross-section satisfy the beam transmission requirements detailed in the previous section, as the beam is transmitted through the transverse section of the sample (perpendicular to the tube length). Moreover, the laser pulse energy and focus position were adjusted to produce a sub-millimetre cavitation bubble, thereby ensuring that the field of view and recording duration met the requirements illustrated in Fig. 4. Figure 5 portrays the final configuration of the sample environment alongside the multi-projection technique.

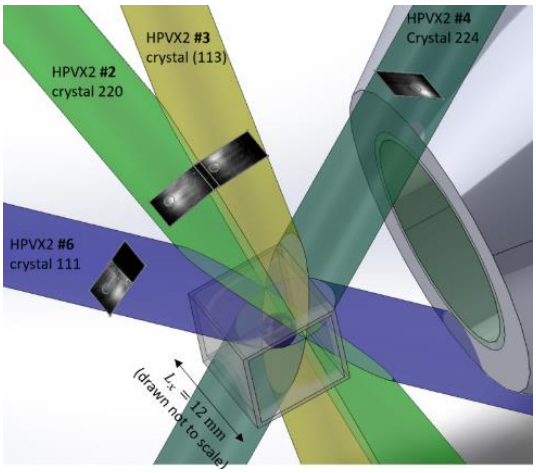

Fig 5. Schematic of the sample environment to validate the MHz-TOMSOCOPY technique.

Results

We used the designed sample environment and experiments to visualise laser-induced cavitation using the MHz-TOMOSCOPY technique. This included over 50 experiments with different cavitation bubble sizes adjusted by changing the laser specifications, aimed at evaluating the effects of laser energy on the cavitation bubble features. Figure 6 illustrates an example of the obtained multi-projection results, using HPVX2 #2 (220 reflection) and HPVX2 #4 (224 reflection) projections shown in Fig. 5, for a cavitation bubble induced by the laser discharge. Here, HPVX2 #2 covers the jet-view, where the beam reflection and camera were aligned with the direction of the microjet, and HPVX2 #4 covers the orthogonal-view with the reflection and camera aligned perpendicular to the jet direction. To quantify the bubble evolution, we calculated the equivalent radius of the spherical bubble in each image, and the results are presented in Fig. 7.

The results show that the laser discharge produces a tiny bubble, presumably containing high-pressure and high-temperature vapour. The high-temperature and high-pressure vapour cause the bubble expansion over time, until the bubble reaches its maximum size of 356 µm at t = 20.4 µs, at which the bubble's internal pressure reaches the saturated pressure, i.e., 2488 Pa, estimated from the NIST database. Following this, as the bubble internal pressure is significantly smaller than the ambient liquid pressure, i.e. 0.1 MPa, the bubble shrinks in size over 20.4 < t < 40.8 µs until it collapses entirely at 40.8 µs. According to the numerical simulations performed during the preliminary studies, a micro-jet forms at the onset of the collapse due to the retarding effects of the wall near the bubble. This high-velocity jet pierces the bubble and reshapes the

bubble into a toroidal-shaped structure, while the bubble expands again following the first collapse, as shown in Fig. 6 (t = 50.5 µs). According to our simulations, the bubble rebounds (re-expands) due to the low-pressure region generated by the spherical shock wave emitted from the first collapse, which nucleates the bubble again. This bubble re-expands until the momentum of the bubble and the ambient fluid are balanced, i.e., t = 55 µs, followed by the bubble collapse at t > 55 µs.

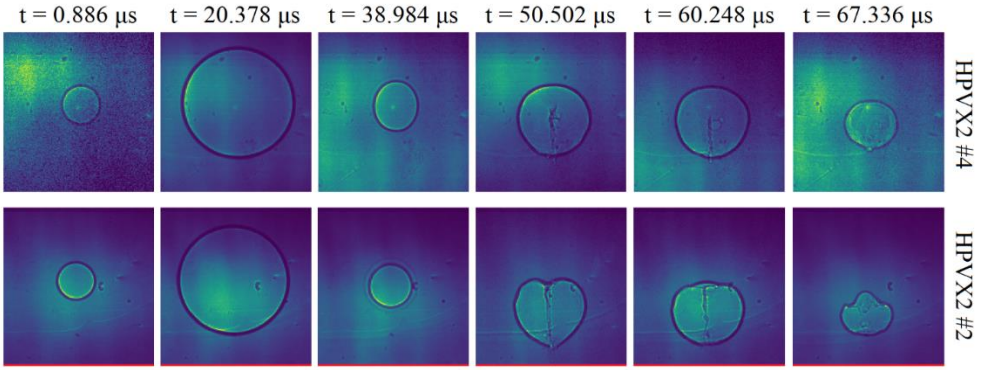

Fig 6. Snapshots of the bubble shape captured by HPVX2 #4 (orthogonal-view) and HPVX #2 (jet-view). The red lines indicate the position of one of the walls.

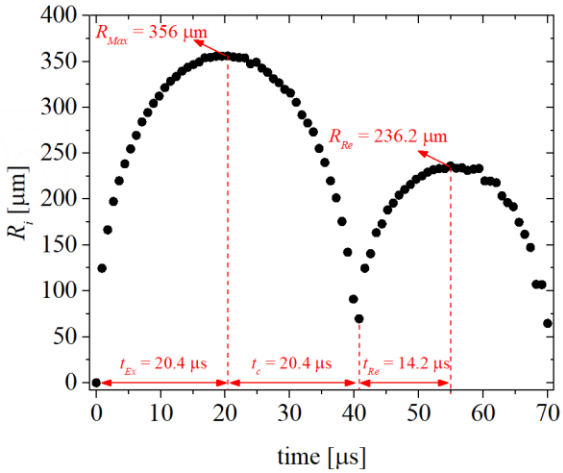

Fig 7. Temporal evolution of the bubble radius. Here, R_{Max} and R_{Re} are the maximum size of the bubble during the expansion and rebound, respectively. Additionally, t_{Ex}, t_c, and t_{Re} are the expansion, collapse, and rebound time scales, respectively.

Conclusions and outlook

In Task 3.4, we defined a set of criteria to design a suitable sample environment and experiments to validate the MHz-TOMSOCOPY technique, while addressing knowledge gaps in the literature on cavitation. The selected criteria included beam transmission, novelty, resolution, and numerical simulation requirements. We performed numerical and experimental (both in-house experiments at the University of Oxford and experiments at the EuXFEL) to evaluate these criteria in different sample environments. Using this approach, we identified laser-induced cavitation as the most suitable sample environment for the technique, with numerous knowledge gaps in this

Funded by
the European Union

field persisting within the fluid dynamics community. The selected sample environment includes a rectangular tube with a small cross-section, ensuring sufficient beam transmission through the sample for the visualisation. We also set the laser energy to produce a cavitation bubble with spatiotemporal characteristics matching the technique's resolutions. These investigations led to new insights into laser-induced cavitation and coherent motions in hydrodynamic cavitation, which were presented in [2] and [3].

Following these preliminary studies, we conducted experiments at EuXFEL using the MHz-TOMOSCOPY technique and quantified the key features of the laser-induced cavitation bubble. The forthcoming tasks beyond this project include reproducing the cavitation bubble features with the numerical solvers developed in this project and comparing the results with the reconstructed data from MHz-TOMOSCOPY. We expect at least an additional publication on this topic by July 2026.

References

[1] C. Brennen, Cavitation and bubble dynamics, Oxford University Press, 1995.

[2] M. Shahsavari, A.M. Korsunsky, H. Soyama, T. Sato, J.C.P. Koliyadu, P. Vagovic, D. Eakins, "On the collapse features of cavitation bubbles near a flat wall: effects of pressure and tandem distribution," *Physics of Fluids*, Vol. 37, 093378, 2025.

[3] M. Shahsavari, D. Eakins, P. Vagovič, H. Soyama, J.C.P. Koliyadu, T. Sato, R. Graceffa, A. Mazzolari, S. Birnšteinová, D. Moško, J. Uličný, W. Yashiro, A. Meents, "Experimental investigation of cavitation dynamics at mesoscale and microscale in swirled and non-swirled venturi tubes," *Physics of Fluids*, in press, 2025.

[4] C.C. Coussios and R.A. Roy, "Applications of acoustics and cavitation to noninvasive therapy and drug delivery," *Annual Review of Fluid Mechanics*, Vol. 40, pp.395–420, 2008.

[5] M.R. Bailey, L.A. Crum, O.A. Sapozhnikov, A.P. Evan, J.A. McAteer, T. Colonius, R.O. Cleveland, "Cavitation in shock wave lithotripsy", *Journal of the Acoustical Society of America*, Vol. 114, pp. 2417–2418, 2003.

[6] R. Zha, D. Wang, C. Wang, Y. Liao, X. Mai, Z. Li, H. Wang, C. Lei, S. Li, S. Liu, X. Wang, "Mechanism of stone suction in thulium laser lithotripsy: Laser-induced cavitation bubble dynamics," *Physics of Fluids*, Vol. 37, 033344, 2025.

[7] M. Zupanc, T. Kosjek, M. Petkovsek, M. Dular, B. Kompare, B. Sirok, Z. Blazeka, E. Heath, "Removal of pharmaceuticals from wastewater by biological processes," *Ultrasonics Sonochemistry*, Vol. 20, pp. 1104–1112, 2013.

[8] Z. Pandur, J. Zevnik, D. Podbevsek, B. Stojkovic, D. Stopar, M. Dular, "Water treatment by cavitation: Understanding it at a single bubble–bacterial cell level," *Water Research*, Vol. 236, 119956, 2023.

[9] H. Soyama and A. Korsunsky, "A critical comparative review of cavitation peening and other surface peening methods," *Journal of Materials Processing Technology*, Vol. 305, 117586, 2022.

[10] D. Ao, Y. Li, C. Liu, Z. Wang, "Study on cavitation flow characteristics of orifice plate–elbow structure in liquefied natural gas receiving station," *Physics of Fluids*, Vol. 37, 096115, 2025.

[11] T. Trummler, S.J. Schmidt, N.A. Adams, "Investigation of condensation shocks and re-entrant jet dynamics in a cavitating nozzle flow by large-eddy simulation," *International Journal of Multiphase Flow*, Vol. 125, 103215, 2020.

[12] W.H. Nurick, “Orifice cavitation and its effect on spray mixing,” *Journal of Fluids Engineering*, Vol. 98, pp. 681–687, 1976.

[13] W. Bergwerk, “Flow pattern in diesel nozzle spray holes,” *Proceedings of the Institution of Mechanical Engineers*, Vol. 173, pp. 655–660, 1959.

[14] H. Shi, X. Wang, Q. Liu, P. Nikrityuk, “The influence of inflow swirls on phases separation in a venturi tube,” *Separation and Purification Technology*, Vol. 281, 119954, 2022.

[15] H. Soyama, “Luminescence intensity of vortex cavitation in a venturi tube changing with cavitation number,” *Ultrasonics Sonochemistry*, Vol. 71, 105389, 2021.

[16] P. Jain, V. Bhandari, K. Balapure, J. Jena, V. Ranade, D. Killedar, “Hydrodynamic cavitation using vortex diode: An efficient approach for elimination of pathogenic bacteria from water,” *Journal of Environmental Management*, Vol. 242, pp. 210–219, 2019.

[17] G. Mancuso, M. Langone, G. Andreottola, “A swirling jet-induced cavitation to increase activated sludge solubilisation and aerobic sludge biodegradability,” *Ultrasonics Sonochemistry*, Vol. 35, pp. 489–501, 2017.

[18] G. Loraine, G. Chahine, C.T. Hsiao, J. Choi, P. Aley, “Disinfection of gram-negative and gram-positive bacteria using dynajets hydrodynamic cavitating jets,” *Ultrasonics Sonochemistry*, Vol. 19, pp. 710–717, 2012.

[19] C. Li and S.E. Ceccio, “Interaction of single travelling bubbles with the boundary layer and attached cavitation,” *Journal of Fluid Mechanics*, Vol. 322, pp. 329–353, 1996.

[20] X. Tian, Z. Li, Z. Qian, “Effect of dissolved air content on attached cavitation in a venturi section,” *Physics of Fluids*, Vol. 37, 013355, 2025.

[21] O. Ram, K. Agarwal, J. Katz, “On the mechanisms that sustain the inception of attached cavitation,” *Journal of Fluid Mechanics*, Vol. 901, A25, 2020.

[22] J. Luo, W. Xu, B.C. Khoo, “Stratification effect of air bubble on the shock wave from the collapse of cavitation bubble,” *Journal of Fluid Mechanics*, Vol. 919, R2, 2021.

[23] G. Xiang, Z. Ren, J. Yang, L. Liu, Z. Zuo, S. Liu, “On the transient dynamics of laser-induced cavitation bubbles near the end of a slender cylinder,” *Physics of Fluids*, Vol. 36, 093349, 2024.

[24] A. Philipp and W. Lauterborn, “Cavitation erosion by single laser-produced bubbles,” *Journal of Fluid Mechanics*, Vol. 361, pp. 75–116, 1998.